Pulsed ultrasound-modulated optical tomography using spectral hole-burning

Youzhi Li, Chulhong Kim, Huiliang Zhang, Kelvin H. Wagner, Philip Hemmer, et al.

Youzhi Li, Chulhong Kim, Huiliang Zhang, Kelvin H. Wagner, Philip Hemmer, Lihong V. Wang, "Pulsed ultrasound-modulated optical tomography using spectral hole-burning," Proc. SPIE 6856, Photons Plus Ultrasound: Imaging and Sensing 2008: The Ninth Conference on Biomedical Thermoacoustics, Optoacoustics, and Acousto-optics, 68561R (28 February 2008); doi: 10.1117/12.774157

SPIE.

Event: SPIE BiOS, 2008, San Jose, California, United States

Pulsed ultrasound-modulated optical tomography using spectral hole-burning

Youzhi Li [a], Chulhong Kim [a], Huiliang Zhang [b], Kelvin H. Wagner [c], Philip Hemmer [b], and Lihong V. Wang [a†]

[a] *Biomedical Engineering Department, Washington University in St Louis, St Louis, MO 63130*

[b] *Electrical and Computer Engineering Department, Texas A&M University, College Station, TX 77843*

[c] *Electrical and Computer Engineering Department, University of Colorado at Boulder, Boulder, CO 80309*

[†]*Correspondence: lhwang@biomed.wustl.edu*

ABSTRACT

We present a novel optical quantum sensor using spectral hole-burning for detecting signals in ultrasound-modulated optical tomography. In this technique, we utilize the capability of sub-MHz spectral filtering afforded by a spectral hole burning crystal to select the desired spectral component from the ultrasound-modulated diffuse light. This technique is capable of providing a large *etendue*, processing a large number of speckles in parallel, tolerating speckle decorrelation, and imaging in real-time. Experimental results are presented.

Keywords: Acousto-optical interaction, ultrasound-modulated optical tomography, spectral-hole burning, spectral filtering, *etendue*.

1. INTRODUCTION

Optical imaging using non-ionizing radiations in biological tissue is highly desirable because the optical properties of biological tissue, such as scattering coefficient and absorption coefficient, in the visible and near infrared region of the electromagnetic spectrum are directly related to the molecular constituents of tissues and the electronic and/or vibrational structures at the molecular level. As consequences, these optical properties (also called optical contrast) are intrinsically sensitive indicators of tissue abnormalities and functions. The hallmarks of cancers include angiogenesis, hyper-metabolism, pleomorphism, and invasion into normal adjacent tissue. Optical properties can be used to quantify these hallmarks and consequently can provide early-cancer detection. Architectural changes at the cellular and sub-cellular levels are revealed in the optical scattering properties, whereas angiogenesis and hyper-metabolism are intrinsic to the optical absorption properties. However, high-resolution optical imaging for greater than ~1 mm in imaging depth is very challenging since biological tissues are turbid media for light transportation.

Pure optical biomedical imaging techniques, such as DOT, suffer from poor spatial resolution caused by the scattering nature of biological tissues. To overcome the strong optical scattering to achieve a good spatial resolution, ultrasonic waves can be employed to localize the optical properties of thick soft tissues[1, 2] for an ultrasonic wave is scattered 2-3 orders of magnitude weaker in soft tissues than an optical wave is. This technique is called ultrasound-

Photons Plus Ultrasound: Imaging and Sensing 2008: The Ninth Conference on Biomedical Thermoacoustics, Optoacoustics, and Acousto-optics, edited by Alexander A. Oraevsky, Lihong V. Wang, Proc. of SPIE Vol. 6856, 68561R, (2008) · 1605-7422/08/$18 · doi: 10.1117/12.774157

modulated optical tomography (UOT),[2, 3] or acousto-optic tomography,[4] which fuses the well-developed ultrasonic technique and the promising optical imaging by employing the acousto-optic interaction effect[2, 4, 5] having advantages of highly desired optical contrast like in DOT and ultrasonic resolution like in sonography. In this technology, a near-infrared coherent laser source illuminates a thick tissue sample while a focused ultrasound wave is launched into the sample through water or ultrasound coupling gels. A portion of the multiply-scattered photons overlapped with the ultrasound field is modulated due to the ultrasound-induced scattering particle displacements and the local refractive index change[6-11] yielding modulation sidebands. The modulation sidebands carry the local optical properties of the tissue sample, while the strong DC term contributes as noise source. By using the photons in these sidebands[3, 12-32], one is able to form a biomedical image with optical contrast and a spatial resolution determined by the parameters of the applied ultrasonic field. Specifically, the lateral resolution is determined by the focal spot size of the ultrasound transducer, and the axial resolution can be achieved by using either frequency-swept ultrasound waves[13] or ultrasound pulses.[1, 33] The detection of the ultrasound-modulated photons in a UOT system is, however, a very demanding task since the modulated photons are usually weak (this is particularly true when high frequency short ultrasound pulses are used to obtain sub-millimeter resolution) and spatially incoherent (speckles).

Different detection approaches have been proposed. A single fast detector was first been used to detect the modulation of the speckle pattern at the applied ultrasonic frequency.[3] The optical etendue ($G = S \cdot \Omega$, defined as the product of the detector active area S and the acceptance solid angle Ω) is limited since only one or a few speckle grains can be detected because the detected modulation depth decreases by $1/\sqrt{N}$ where N is the number of the speckle grains.[4] A confocal Fabry-Perot interferometer (CFPI) has been employed filtering the one sideband of the ultrasound-tagged photons from the UOT signals while suppressing the DC and the other modulation sideband.[24] This technique also suffers from a small *etendue*. Multi-pixel CCD detection schemes,[14-16, 18, 20-23, 34] which are based on monitoring speckle changes when a ultrasound field is turned on and off, provide a better *etendue* but may not be applicable to *in vivo* imaging scenarios due to the slow CCD frame rates and the fast decorrelation rate of the speckles. The photorefractive effect afforded by photorefractive crystals has recently been adopted to interferometrically detect the ultrasound-modulated photons in UOT.[25-32] These techniques usually utilize bismuth silicon oxide crystals for their large gain and relatively fast response time, and offer a larger etendue over the afore-mentioned detection approaches. Yet, the applicability is limited by the response time, $\tau_{PR} \approx 100$ ms, of the photorefractive crystals since speckle patterns generated by an *in vivo* biological tissues usually have a decorrelation time less than 1 ms because of the fast Brownian motion. The lack of efficient detection mechanism has so far prevented this promising modality from being developed into a reliable system for research and clinical purposes.

2. MOTIVATIONS OF USING SPECTRAL-HOLE BURNING

To attack the detection difficulty in UOT, we will employ spectral-hole burning (SHB) technique as a front-end quantum filter to efficiently detect the ultrasound modulated photons, which functions as a sub-MHz bandpass absorption filter.

SHB has been extensively investigated for various different applications, including data storage,[35, 36] RF spectrum analysis,[37, 38] LIDAR sensing and signal processing.[39] A SHB medium is a rare-earth ion doped inhomogeneously broadened optical absorber, which can be modeled as a two level system.[40] When cryogenically-cooled, it has a sub-MHz homogeneous linewidth $\Delta\Gamma_H$ and an inhomogeneous bandwidth $\Delta\Gamma_I$ of GHz.[41] As schematically shown in Fig. 1, each homogeneous frequency can be individually accessed using a proper narrow laser line excitation. When a monochromatic laser source at frequency f_L illuminates a cryogenically-cooled SHB crystal, the resonant ions are excited from their ground

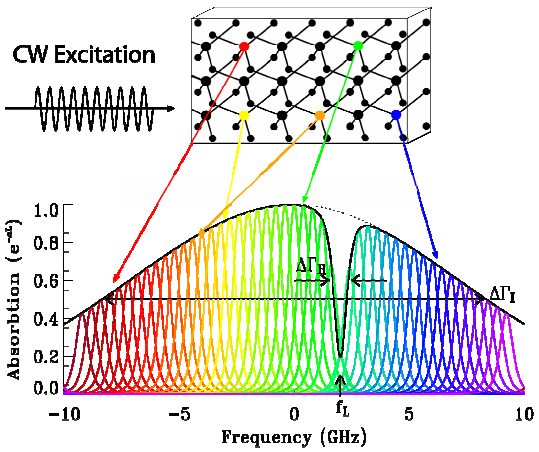

Fig. 1 Simulated spectral absorption profile of a SHB crystal with a spectral hole burned at f_L. $\Delta\Gamma_I$: bandwidth of the crystal. $\Delta\Gamma_H$: homogeneous linewidth of the doped ions.

states to the excited states. Sufficiently intense illumination excites nearly all of the resonant ions, and as a consequence, a spectral hole is engraved at f_L with linewidth of $\Delta\Gamma_H$ in the spectral absorption band of the crystal, resulting in a narrowband spectral transparency at f_L. For an optically dense SHB crystal ($\alpha(f\neq f_L)L_c>>1$, where L_c is the crystal thickness), a deep spectral hole engraved at f_L will significantly reduce the absorption coefficient $\alpha(f_L)$, yielding a transparency at this particular frequency, yet $\alpha(f\neq f_L)$, will stay unchanged, leaving the crystal in a highly absorptive state across the bandwidth of $\Delta\Gamma_I$ other than f_L. This allows us to perform absorption-based spectral filtering in parallel. This feature is ideal for detecting the US-modulated photons in a UOT system. The transmitted UOT spatial speckles have the DC light suppressed so that they can simply be incoherently integrated to achieve a high signal-to-noise-ratio.

Furthermore, the SHB technique has a potential for a huge optical *etendue*. In principle, the acceptance angle of our proposed absorption-based quantum filter can be nearly 2π, yielding an *etendue* at 1131 *sr mm*^{2} for a 10×9 mm crystal aperture, which is about 3 orders of magnitude improvement over the existing photorefractive methods. Since this system is based on a frequency-dependent absorption filtering, it is inherently insensitive to speckle decorrelation, potentially allowing *in vivo* biomedical imaging.

The features of spectral hole-burning based ultrasound-modulated optical tomography (SHB UOT), including DC suppression, parallel speckle processing, large *etendue*, and immunity to speckle deccorelation, open an opportunity to us to develop the proposed system into a reliable and clinically applicable optical imaging modality for breast cancer screening, a fundamental breakthrough.

3. Pulsed ultrasound-modulated optical tomography using spectral-hole burning as spectral filtering

When a coherent light with frequency of ω_0 interacts with an ultrasound wave with a frequency of ω_u inside a biological tissue, the amplitude of the nth independent optical speckle caused by the tissue can be expressed in phase modulation as

$$E_n(r,t) \propto A_n \exp\left(j\left(\omega_0 t + m\sin(\omega_u t) + \phi_n(r,t)\right)\right) \tag{1}$$

Where, A_n is a constant, m is the modulation depth, $\phi_n(r,t)$ is a random phase. For a weak modulation, Eq. (1) can be approximated as

$$E_n(r,t) \propto A_n \exp\left(j\varphi_n(r,t)\right)\left(\exp(j\omega_0 t) \pm \frac{m}{2}\exp\left(j(\omega_0 \pm \omega_u)t\right)\right) \tag{2}$$

which represents an unmodulated DC light at ω_0 and two modulation sidebands at $(\omega_0 \pm \omega_u)$ induced by the ultrasound wave at ω_u.

By employing the SHB technique, one can create a bandpass filtering with a sub-MHz bandwidth to pass one of the two modulation sidebands while suppressing the unmodulated DC and the other sideband, yielding ideally either the up-shifted sideband at $(\omega_0 + \omega_u)$ or the down-shifted sideband at $(\omega_0 - \omega_u)$ depending the frequency of the created filter. The transmitting field can thus be either

$$E_n(r,t) \propto A_n \exp\left(j\varphi_n(r,t)\right)\left(\frac{m}{2}\exp\left(j(\omega_0 + \omega_u)t\right)\right) \tag{3a}$$

or

$$E_n(r,t) \propto A_n \exp\left(j\varphi_n(r,t)\right)\left(\frac{m}{2}\exp\left(j(\omega_0 - \omega_u)t\right)\right) \tag{3b}$$

Consequently, the filtered speckles can be incoherently integrated using a large area square-law detector, yielding

$$i_{uot} \propto \sum_n^N \frac{A_n^2 m^2}{4} \tag{4}$$

where N is the number of the detected speckles. The signal-to-noise ratio of this signal can thus be improved by $\sqrt{N}$ as N increases. This signal carries the spatial information determined by the ultrasound parameters, and can be used to form images as described below.

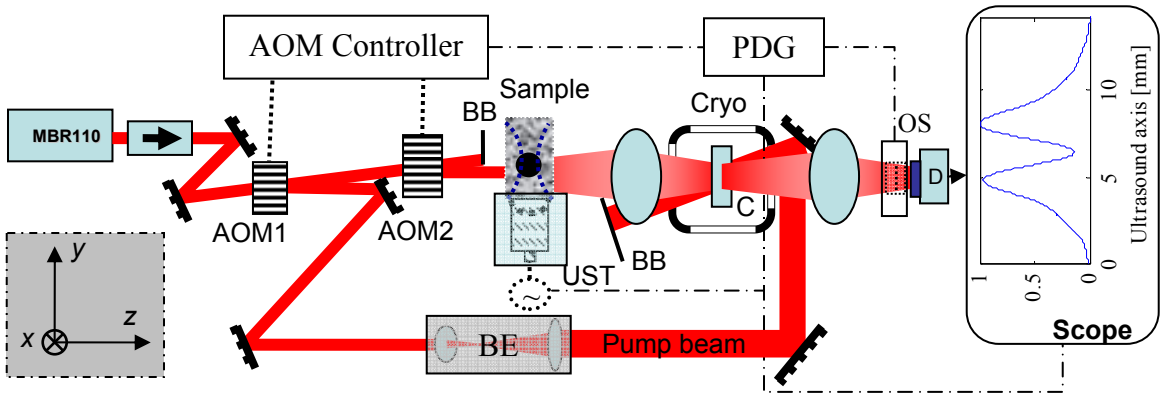

Fig. 2. Experimental setup of the SHB UOT. AOM: acousto-optic modulator. UST: ultrasound transducer. Cryo: cryostat. C: crystal. BB: beam block. BE: beam expander. D: detector. OS: optical shutter. **Left bottom inset:** lab coordinates: *x – sample scanning direction; y – ultrasound propagation direction; z – light propagation direction.*

The present SHB UOT system is schematically shown in Fig. 2. The SHB crystal we used in our current system is a 10×9×1.5 mm^3 2%@Tm^{3+}:YAG crystal. Its working wavelength at 793 nm is a preferred wavelength for biomedical imaging, and solid state laser sources at this wavelength are readily available. The optical absorption length is measured as $\alpha(f)L_c$=4. A CW Ti:Sapphire laser (Coherent MBR110), pumped by a frequency-doubled diode laser (Coherent Verdi 10 W), is utilized as the laser source, which is tuned to operate at 793.38 nm with an output of 2 W. The laser beam is first frequency-shifted by 70 MHz with an acousto-optic modulator (AOM) labeled as AOM1 in Fig. 2 (IntraAction, Model: AOM802A1) driven by one channel of a dual channel frequency synthesizer (IntraAction, Model: DFE-754A4-16). The synthesizer is amplitude-modulated by 3.3 ms, 0.98 V pulses generated by a function generator (Stanford Research, Model: DS345), yielding 980 mW, 3.3 ms long, 70 MHz frequency-shifted optical pulses. The 70 MHz frequency-shifted pulses are used as the pump beam as shown in Fig. 2, which is beam expanded to cover the 9 mm diameter clear aperture of the crystal. The crystal is cryogenically cooled to ~4 K with a cryostat (Janis, Model: STVP-400). The pump beam burns transparent spectral holes across the crystal's clear aperture, forming a number of narrowband bandpass filters, which have a life time of about 10 ms. These filters are employed to process the ultrasound-modulated diffuse speckles in parallel.

After the narrowband bandpass filters are engraved, the AOM1 is turned off and another AOM of the same model, AOM2, is turned on with a driven frequency at 75 MHz, equivalent to the AOM1 driven frequency plus the ultrasound frequency of 5 MHz. The light pulse, which is 20 μs long and has 500 mW peak power, diffracted off the AOM2 is beam-shaped to a 0.3 mm × 8 mm elliptical beam to illuminate the 50 × 50 × 10 mm tissue-mimicking phantom sample. The sample consists of 10% porcine skin gelatine (Sigma G2500) and 1% Intralipid, yielding a reduced scattering coefficient of $\mu_s' \approx 7\,\mathrm{cm}^{-1}$ at the optical wavelength of 793 nm. A 2-cycle 5 MHz ultrasound pulse with a peak pressure of 4.3 MPa, is simultaneously launched into the sample through water using a focusing transducer (Panametrics-NDT, Model: A326S-SU, focal length: 16.2 mm, focal spot size: 0.5 mm). The ultrasound pulse has a mechanical index (defined as the ratio of the ultrasound peak pressure in MPa to the square root of its central frequency in MHz) of 1.9, which is also within the ultrasound safety limit.[42] The ultrasound pulse forms a volumetric ultrasonic field of 0.12 mm^3 (ultrasound speed in tissue =1.5 mm/μs) in the transducer focal zone, determining the optimum resolution of the final tomograms. The multiply scattered light distributed along the ultrasound propagation direction is modulated by this ultrasound volume as the ultrasound propagates through the sample, allowing the creation of a spatial map of the optical properties of the sample along the ultrasound path (the so-called A-line) as shown in Fig. 2 scope trace, which is synchronized with the AOM2. The dip corresponds to the position of an absorber buried inside the sample.

The acousto-optic interaction yields two primary weak sidebands at 70 MHz and 80 MHz in addition a strong un-modulated DC speckle field. The ultrasound-modulated diffuse light is passed through the SHB crystal, where the 70 MHz spectral filters. The spectral filters transmit the sideband of 70 MHz while significantly attenuating the strong un-

modulated DC and the other sideband at 80 MHz. The transmitted speckles are detected using a large area Si detector (Thorlabs PDA55). An optical shutter (Uniblitz VS14S2S1) is employed in front of the detector to time-gate the pump beam from the detector to avoid detector saturation caused by the scattered pump beam. The timing sequence of the system is controlled with a pulse delay generator (Stanford DG535) as shown by the dash-dot lines in Fig. 2.

4. EXPERIMENTAL RESULTS

We first characterized the spectral filtering capability of the SHB crystal used in our experiments by measuring its signal absorption after the crystal was cooled down with the pump beam turned on and off. First, the pump beam was turned off, meaning no spectral filters would be engraved. The transmitted light was measured at room temperature and at 4 K. The differential between these two measurements gives the DC suppression as governed by Beer's law $I_{out} \approx I_{in} \exp(-\alpha L_c) = I_{in} \exp(-4)$, resulting in a DC suppression of 18 dB. It should be pointed out that the DC suppression can be significantly improved provided an optically thicker crystal ($\alpha L_c >> 4$) is used. The pump beam was then turned on at 4 K, engraved transparent spectral filters at the desired frequency. The engraved spectral filters substantially improve the light transmission at the corresponding frequency, while blocking light at all other frequencies. 14 dB transmission improvements have been observed. The FWHM of the transmission peak, the bandwidth of the spectral filter, was measured at about 710 KHz.

To verify its capability of processing a large number of speckles in parallel, we need to find the relationship between the signal strength and the number of the speckles being filtered. To do so, the pump beam size was controlled using an iris. The ultrasound-modulated diffused speckles covered the whole aperture of the crystal. Thus, by enlarging the pump beam, the number of the speckles being processed would increase, the UOT signal should be consequently strengthened. Fig. 3 depicts the signal growth as a function of the pump beam size, in which the circles are the measured values, and the error bars are standard deviations. The solid line is shape preserved fitting. It can be seen from the curve that the signal does initially grow nearly linearly as the pump beam is enlarged, and then the signal growth slows down as the pump beam size is further increased. This may be mainly due to two reasons: 1. The modulated-light may not be fully diffused since the sample is thin. 2. The pump beam obeys a Gaussian distribution as verified by measuring its total power as a function of the beam area. The Gaussian distributed pump beam burns shallower holes at its edge, yielding weaker signals. For a fully developed speckle pattern and a uniform pump beam, we may expect that the curve in Fig. 3 obey a linear relationship over a larger area.

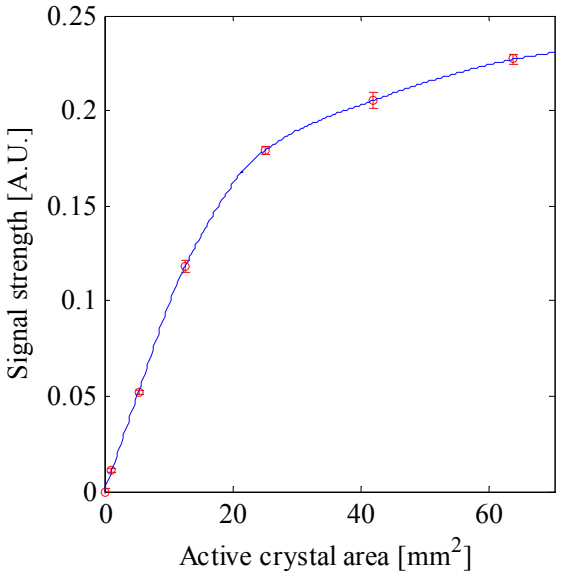

Fig. 3. **Parallel speckle pattern processing**. UOT signal (circles) as a function of the pump beam size. The error bars are the standard deviations. The solid line is the shape preserved fitting.

Tomographic imaging experiments have been carried out. Fig. 4 shows two of our imaging results. Two small rectangular optical absorber (Black India Ink) was buried in the middle of a 50 × 50 × 10 (x × y × z) mm phantom to mimic the optical absorption of a soft tissue as shown in Fig. 4 (a). The dimensions of the left absorber were 2.8 × 1.8 × 0.8 mm and the right absorber were 2.8 × 1.3 × 0.8 mm, respectively. And the gap between the absorbers was about 7.5 mm. In the experiment, the ultrasound transducer and the sample illuminating light were fixed. And the phantom was scanned along x-axis for 14.25 mm with a step size of 0.375 mm. The tomogram was interpolated. It can be seen from Fig. 4 (b) that the absorber was imaged with high fidelity with only 64 times averaging. The typical A-lines of the present pulsed SHB UOT are shown in Fig. 4 (c). The solid line is the A-line when no absorber is within the field of

view corresponding to the black solid line in Fig. 4 (b), whereas the dashed line, corresponding to the dashed line in Fig. 4 (b), presents an A-line with an absorber at the center of the field of view, the dip indicates the position of the absorber.

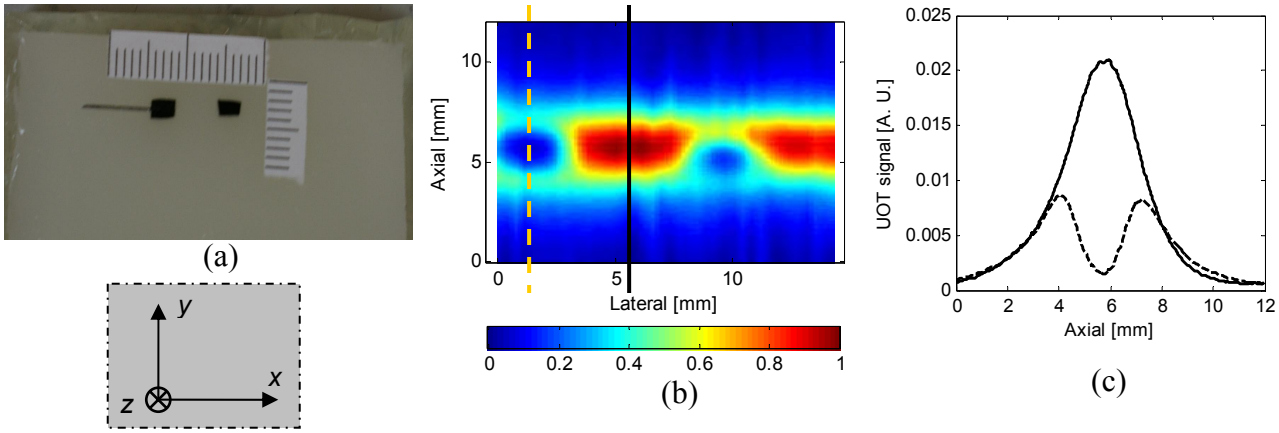

Fig. 4. SHB UOT images. (a). The photograph of the optical absorber buried inside the scattering medium (cannot be seen from the outside). (b). B-mode tomogram with 64 averages. (c). typical A-lines of the pulsed SHB UOT, corresponding to the dashed and solid lines in (b), respectively. **Left bottom inset:** lab coordinates

Imaging speed of the SHB UOT can be further improved by reducing average times. It has been demonstrated that an imaging speed of 80 μs / A-line can be achieved with a fair image quality as to be reported somewhere else. For this imaging speed, the optical power for each A-line imaging location is well below the ANSI laser safety limit at 793 nm.[43]

5. DISCUSSIONS AND CONCLUSIONS

The large optical *etendue* is one of the primary advantages of our system. As mentioned above, since the acceptance angle of our absorption-based quantum filter can be nearly 2π, a 10×9 mm crystal can thus have an ideal *etendue* of 1131 *sr mm*^{2}. In our current system, the effective *etendue* for this front-end filter is calculated as 31 *sr mm*^{2}, limited by the numerical aperture of our cryostat windows. Yet this *etendue* is already an order of magnitude improvement over the photorefractive crystal based technique,[32] and more than two orders of magnitude improvement over the CFPI.[24] However, the *etendue* of our system can be further improved by increasing the numerical aperture of the cryostat.

In summary, a novel nonlinear optical quantum filter afforded by a SHB crystal for detecting US-modulated signals in a UOT system has been demonstrated. It processes multiple speckles in parallel and has the largest *etendue* comparing with other existing UOT techniques. Since this technique is based on frequency-dependent absorption, it is inherently insensitive to fast speckle decorrelation, potentially allowing *in vivo* imaging, a fundamental breakthrough. In addition, the speed advantage of our technique offers potential for real-time image. In our proof-of-feasibility experiments, we imaged tissue-mimic phantoms with 10 mm thickness. It should be pointed out immediately that this is not the limit to our technique since the imaging depth may be easily improved without sacrificing the imaging speed by utilizing a thicker crystal to further suppress the strong DC and a balanced detection scheme[44] to reject laser intensity noise. Furthermore, the imaging depth and the resolution of our technique are scalable by simply employing different ultrasound frequency. This technique opens an opportunity to develop a reliable optical imaging system with a scalable ultrasound resolution for various biomedical applications such as early breast cancer detection.

ACKNOWLEDGEMENT

This is work is supported by US National Institute of Health, grant #: R33 CA 094267**.**

REFERENCES

[1] Marks, F. A., Tomlinson, H. W. and Brooksby, G. W., "A comprehensive approach to breast cancer detection using light: photon localization by ultrasound modulation and tissue characterization by spectral discrimination," Proc. SPIE **1888**, 500-510 (1993).
[2] Leutz, W. and Maret, G., "Ultrasonic modulation of multiply scattered light," Physica B **204**, 14-19 (1995).
[3] Wang, L. V., Jacques, S. L. and Zhao, X., "Continuous-wave ultrasonic modulation of scattered laser light to image objects in turbid media," Opt. Lett. **20**, 629-631 (1995).
[4] Kempe, M., Larionov, M., Zaslavsky, D. and Genack, A. Z., "Acousto-optic tomography with multuply scattered light," JOSA A **14**, 1151-1158 (1997).
[5] Mahan, G. D., Engler, W. E., Tiemann, J. J. and Uzgiris, E., "Ultrasonic tagging of light: theory," PNAS **95**, 14015-14019 (1998).
[6] Wang, L. V., "Mechanisms of ultrasonic modulation of multiply scattered coherent light: a Monte Carlo model," Opt. Lett. **26**, 1191-1193 (2001).
[7] Wang, L. V., "Mechanisms of ultrasonic modulation of multiply scattered coherent light: an analytic model," Phys. Rev. Lett. **87**, 043903 (2001).
[8] Sakadžić, S. and Wang, L. V., "Ultrasonic modulation of multiply scattered coherent light: An analytical model for anisotropically scattering media," Phys. Rev. E **66**, 026603 (2002).
[9] Sakadžić, S. and Wang, L. V., "Modulation of multiply scattered coherent light by ultrasonic pulses: An analytical model," Phys. Rev. E **72**, 036620 (2005).
[10] Sakadžić, S. and Wang, L. V., "Correlation transfer and diffusion of ultrasound-modulated multiply scattered light," Phys. Rev. Lett. **96**, 163902 (2006).
[11] Sakadžić, S. and Wang, L. V., "Correlation transfer equation for multiply scattered light modulated by an ultrasonic pulse," JOSA A **24**, 2797-2806 (2007).
[12] Lev, A., Kotler, Z. and Sfez, B. G., "Ultrasound tagged light imaging in turbid media in a reflectance geometry," Opt. Lett. **25**, 378-380 (2000).
[13] Wang, L. V. and Ku, G., "Frequency-swept ultrasound-modulated optical tomography of scattering media," Opt. Lett. **23**, 975-977 (1998).
[14] Yao, G., Jiao, S. and Wang, L. V., "Frequency-swept ultrasound-modulated optical tomography in biological tissue by use of parallel detection," Opt. Lett. **25**, 734-736 (2000).
[15] Lévêque, S., Boccara, A. C., Lebec, M. and Saint-Jalmes, H., "Ultrasonic tagging of photon paths in scattering media: parallel speckle modulation processing," Opt. Lett. **24**, 181-183 (1999).
[16] Lévêque-Fort, S., "Three-dimensional acousto-optic imaging in biological tissues with parallel signal processing," Appl. Opt. **40**, 1029-1036 (2001).
[17] Lévêque-Fort, S., Selb, J., Pottier, K. and Boccara, A. C., "In situ local tissue characterization and imaging by backscattering acousto-optic imaging," Opt. Comm. **196**, 127-131 (2001).
[18] Li, J., Ku, G. and Wang, L. V., "Ultrasound-modulated optical tomography of biological tissue by use of contrast of laser speckles," Appl. Opt. **41**, 6030-6035 (2002).
[19] Li, J. and Wang, L. V., "Methods for parallel-detection-based ultrasound-modulated optical tomography," Appl. Opt. **41**, 2079-2084 (2002).
[20] Gross, M., Goy, P. and Al-Koussa, M., "Shot-noise detection of ultrasound-tagger photons in ultrasound-modulated optical imaging," Opt. Lett. **28**, 2482-2484 (2003).
[21] Atlan, M., Forget, B. C., Ramaz, F., Boccara, A. C. and Gross, M., "Pulsed acousto-optic imaging in dynamic scattering media with heterodyne parallel speckle detection," Opt. Lett. **30**, 1360-1362 (2005).
[22] Hisaka, M., "Ultrasound-modulated optical parallel speckle measurement with stroboscopic illumination in a coaxial reflection system," Appl. Phys. Lett. **88**, 033901 (2006).
[23] Zemp, R., Sakadžić, S. and Wang, L. V., "Stochastic explanation of speckle contrast detection in ultrasound-modulated optical tomography," Phys. Rev. E **73**, 061920 (2006).
[24] Sakadžić, S. and Wang, L. V., "High-resolution ultrasound-modulated optical tomography in biological tissues," Opt. Lett. **29**, 2770-2772 (2004).
[25] Murray, T. W. et al., "Detection of ultrasound-modulated photons in diffuse media using the photorefractive effect," Opt. Lett. **29**, 2509-2511 (2004).
[26] Ramaz, F. et al., "Photorefractive detection of tagged photons in ultrasound modulated optical tomography of thick biological tissues," Opt. Expr. **12**, 5469-5474 (2004).
[27] Blonigen, F. J. et al., "Computations of the acoustically induced phase shifts of optical paths in acoustophotonic imaging with photorefractive-based detection," Appl. Opt. **44**, 3735-3746 (2005).

[28] Bossy, E., Sui, L., Murray, T. W. and Roy. R. A., "Fusion of conventional ultrasound imaging and acousto-optic sensing by use of a standard pulsed-ultrasound scanner," Opt. Lett. **30**, 744-746 (2005).
[29] Gross, M. et al., "Theoretical description of the photorefractive detection of the ultrasound modulated photons in scattering media," Opt. Expr. **13**, 7097-7112 (2005).
[30] Sui, L., Roy, R. A., DiMarzio, C. A. and Murray, T. W., "Imaging in diffuse media with pulsed-ultrasound-modulated light and the photorefractive effect," Appl. Opt. **44**, 4041-4048 (2005).
[31] Bossy, E., Funke, A. R., Daoudi, K. and Boccara, A. C., "Transient optoelastography in optically diffusive media," Appl. Phys. Lett. **90**, 174111 (2007).
[32] Xu, X. et al., "Photorefractive detection of tissue optical and mechanical properties by ultrasound modulated optical tomography," Opt. Lett. **32**, 656-658 (2007).
[33] Lev, A. and Sfez, B. G., "Pulsed ultrasound-modulated light tomography," Opt. Lett. **28**, 1549-1551 (2003).
[34] Gross, M. et al., "Heterodyne detection of multiply scattered monochromatic light with a multipixel detector," Opt. Lett. **30**, 1357-1359 (2005).
[35] Mossberg, T. M., "Time-domain frequency-selective optical storage," Opt. Lett. **7**, 77-79 (1982).
[36] Renn, A., Wild, U. P. and Rebane, A., "Multidimensional holography by persistent spectral hole burning," J. Phys. Chem. A **106**, 3045-3060 (2002).
[37] Ménager, L., Lorgeré, I., Le-Gouët, J.-L., Dolfi, D. and Huignard, J.-P., "Demonstration of a radio-frequency spectrumanalyzer based on spectral hole burning," Opt. Lett. **26**, 1245-1247 (2001).
[38] Colice, M., Schlottau, F. and Wagner, K. H., "Broadband radio-frequency spectrum analysis in spectral-hole-burning media," Appl. Opt. **45**, 6393-6408 (2006).
[39] Li, Y. et al., "Ultrawideband coherent noise lidar range-Doppler imaging and signal processing by use of spatial-spectral holography in inhomogeneously broadened absorbers," Appl. Opt. **45**, 6409-6420 (2006).
[40] Allen, L. and Eberly, J. H., [Optical resonance and two-level atoms], Dover publications, Inc., New York, 1987.
[41] Sun, Y., Thiel, C. W., Cone, R. L., Equall, R. W. and Hutcheson, R. L., "Recent progress in developing new rare earth materials for hole burning and coherent transient applications," J. of Lumin. **98**, 41-44 (2002).
[42] Dalecki, D., "Mechanical bioeffects of ultrasound," Annu. Rev. Biomed. Eng. **6**, 229-248 (2004).
[43] [American national standard for the safe use of lasers, Standard Z136.1-2000], ANSI, Inc., New York, 2000.
[44] Hobbs, P. C. D., "Ultrasensitive laser measurements without tears," Appl. Opt. **36**, 903-920 (1997).